

Intra-class Variation Isolation in Conditional GANs

Richard T. Marriott
Ecole Centrale de Lyon
Ecully, France

richard.marriott@ec-lyon.fr

Sami Romdhani
IDEMIA
Courbevoie, France

sami.romdhani@idemia.com

Liming Chen
Ecole Centrale de Lyon
Ecully, France

lchen@ec-lyon.fr

Abstract

Current state-of-the-art conditional generative adversarial networks (C-GANs) require strong supervision via labeled datasets in order to generate images with continuously adjustable, disentangled semantics. In this paper we introduce a new formulation of the C-GAN that is able to learn realistic models with continuous, semantically meaningful input parameters and which has the advantage of requiring only the weak supervision of binary attribute labels. We coin the method intra-class variation isolation (IVI) and the resulting network the IVI-GAN. The method allows continuous control over the attributes in synthesised images where precise labels are not readily available. For example, given only labels found using a simple classifier of ambient / non-ambient lighting in images, IVI has enabled us to learn a generative face-image model with controllable lighting that is disentangled from other factors in the synthesised images, such as the identity. We evaluate IVI-GAN on the CelebA and CelebA-HQ datasets, learning to disentangle attributes such as lighting, pose, expression and age, and provide a quantitative comparison of IVI-GAN with a classical continuous C-GAN.

1. Introduction

Advances in deep learning have led to the performance of deep neural networks surpassing human levels in a number of tasks, e.g. face-recognition (FR) [14]. One of the most important aspects limiting further progress is the lack of availability of balanced datasets. FR datasets must contain images of many identities in order that networks be able to learn mappings that generalise well to identities not present in the training dataset. They must also contain many images of each identity under a variety of conditions to allow the network to learn robustness to this intra-class variation; i.e. to factors such as pose, expression, lighting, etc. In many FR datasets the intra-class variation is not sufficient and subjects at extreme poses or under harsh lighting conditions may not be recognised [14]. In this paper we present a



Figure 1. Images generated by IVI-GAN using only our novel additive lighting constraint. Left-hand column: $\rho = \mathbf{0}^9$ (ambient); the second, third and fourth columns show the effect of assigning large values to a selection of individual lighting parameters. Results in each column share the same set of lighting parameters.

method of synthesising realistic images that may be used to augment existing datasets. We use a conditional generative adversarial network (C-GAN) [17] to generate new identities and can manipulate image attributes separately and continuously with only the weak supervision of binary attribute labels; e.g. “ambient lighting / non-ambient lighting”.

Generative Adversarial Networks (GANs) [11] are capable of generating highly realistic synthetic data-samples that are almost indistinguishable from samples of real data. This capability is a direct result of the insightful training objective of the generative network: to produce synthetic data that cannot be distinguished from the real thing by a second adversarial network aiming to classify samples as either real

or fake. Recent advances such as use of the Wasserstein loss [1] and various forms of regularisation [13, 18, 4] and training techniques [15] mean that training of GANs is now stable enough to generate data-samples with thousands of dimensions. For example, deep convolutional GANs (DC-GANs) can now produce convincing images at mega-pixel resolution or higher [15, 3].

While classical DC-GANs can generate realistic images, the precise form of these images cannot be easily controlled. The subject of the images is dependent in some way on the values of the random input vector, but *a priori* we do not know in what way. The obvious solution to this problem is the C-GAN, in which the GAN’s discriminator is trained to distinguish *real image+label* pairs from *fake image+parameter* pairs¹. In this way, given some parameter value, the generator is obliged to produce an image that would match the label of equivalent value in order that the “*fake image+parameter*” pair be indistinguishable from a “*real image+label*” pair. Insofar as they go, these conditional formulations prove successful. However, the C-GAN does not take advantage of the main strength of GANs: namely, the ability to learn realistic models directly from data in an unsupervised fashion. In its typical form, a *continuous* C-GAN would require strong supervision via a set of labels. Previous works have conditioned on pose labels and expression action unit magnitudes [22]. The annotation of lighting conditions, however, is notoriously difficult [2]. In this paper we propose a new formulation of the continuous conditional GAN which avoids the need to precisely label data and instead relies only on the weak supervision of simple binary labels. We coin the method *intra-class variation isolation* (IVI) (pronounced as “ivy”) and the resulting network the *IVI-GAN*.

Our contributions are

- A novel continuous conditional GAN formulation that imposes semantic meaning on sets of input parameters without the need for real-valued continuous training labels: the IVI-GAN;
- A thorough evaluation of IVI-GAN including a quantitative comparison with a standard continuous conditional GAN;
- A novel, physically motivated generator constraint to enforce separation of lighting variation from identity in C-GANs;
- An evaluation of state-of-the-art GAN-training methods.

The rest of the paper is organised as follows: In Section 2 we discuss related work; in Section 3 we formalise our

¹N.B. the fake image is dependent on the parameter and the parameters are sampled randomly from the distribution of labels during training of the GAN.

novel continuous conditional GAN formulation; in Section 4 we give details of our implementation; and in Section 5 we present an analysis of results produced using the IVI-GAN.

2. Related Work

Our ultimate goal is to synthesise new training data to improve the training of facial recognition networks. GANs are ideally suited to this task since they are able to synthesize images that are indistinguishable from real training images.

In [23] a C-GAN is used to synthetically augment FR datasets with some success. Their network can generate and modify images of identities in their training dataset or synthesise new identities. (Most other similar work in the literature relies on encodings of input images as the GAN’s source of identity information [22, 2].) Our main concern with [23] is that the network relies entirely on the capability of its auxiliary identity-classifier in order to separate the encoding of identity information and non-identity information. Any residual identity information not captured by the classifier will become encoded by the conditioning vector. This may limit the usefulness of the method for augmenting FR datasets. IVI-GAN, on the other hand, only isolates non-identity information that is labelled as being present in the image, and there is no particular reason why this information should be correlated with identity.

Another method with similar objectives is [8]. In this work the GAN’s generator is trained as a siamese network in which two images are generated from the same random “identity” vector but from different random “observation vectors”. The GAN’s discriminator then decides if the pair of images looks real compared pairs of real training images depicting the same identity but in different situations. Again, the network relies on the discriminator’s capacity to learn to match identities between images in order to separate identity information from extraneous information. There is nothing preventing residual identity information from becoming encoded in the observation vectors.

In [2], synthetic images are generated by combining the identity from one input image with the situational factors of a second image that could be an image of a different person. They essentially implement an AC-GAN trained on images with associated ID labels. However, the generated image is forced to contain the situation factors of the second input image via a pixel-wise reconstruction loss. This pixel-wise loss between two images potentially containing different identities seems to cause generated images to be somewhat blurry. The method also doesn’t allow for the generation of new synthetic identities nor allow control over image attributes without having an example input image.

Various other works use C-GANs to manipulate input images. For example, [7, 12, 6, 24] can each influence various image attributes such as expression or hair colour. How-

ever, without having very precise labels, they do not allow fine-grained control over these attributes, e.g. the intensity of an expression. One recent work that does allow this is [22] in which a C-GAN is trained on a database of images labelled with continuous expression action unit magnitudes (AUs) [10]. Unlike IVI-GAN, this work is dependent on the set of precise continuous valued labels. IVI-GAN requires only binary labels, e.g. neutral / non-neutral expression.

3. Intra-class variation isolation

Before describing intra-class variation isolation, we introduce the conditional GAN. Our best results are achieved using Wasserstein GANs and so we present this version.

3.1. Conditional GANs

A conditional GAN (C-GAN) [17] consists of two networks that are trained alternately: the discriminator, D , is trained to discriminate fake images from real ones; and the generator, G , is trained to generate images that will better fool the discriminator. The function that is minimised in order to train the discriminator is

$$\mathcal{L}_{\theta_D} = \mathbb{E}_{(\mathbf{x}, \mathbf{y}) \sim p_{data}} [D(\mathbf{x}, \mathbf{y}; \theta_D)] - \mathbb{E}_{\mathbf{z} \sim \mathcal{N}, \boldsymbol{\rho} \sim p_{data}} [D(G(\mathbf{z}, \boldsymbol{\rho}; \theta_G), \boldsymbol{\rho}; \theta_D)] \quad (1)$$

where \mathbf{x} is an image and $\mathbf{y} \in \mathbb{R}^n$ an associated vector of labels drawn from the distribution of real data; $\mathbf{z} \in \mathcal{N}^m$ is a random Gaussian vector but could alternatively be drawn from any other real-valued distribution; $\boldsymbol{\rho} \in \mathbb{R}^n$ is a vector of labels used to condition the generator and is usually selected at random from the training dataset; and θ_D and θ_G are the parameters of the discriminator and generator networks respectively. In the Wasserstein GAN, the output of D is a single unbounded scalar value; i.e. no *squashing-function* is applied. Provided that D remains k -Lipschitz continuous, minimising equation (1) with respect to θ_D yields an estimator of the Wasserstein distance (to a scalar, k) between the distributions of real labeled data and $\boldsymbol{\rho}$ -parameterised generated data [1]. Lipschitz continuity is usually achieved by adding an additional *gradient-penalty* term [13] to the discriminator loss in equation (1).

The trained discriminator is then used as the generator loss and equation (2) is minimised with respect to θ_G .

$$\mathcal{L}_{\theta_G} = \mathbb{E}_{\mathbf{z} \sim \mathcal{N}, \boldsymbol{\rho} \sim p_{data}} [D(G(\mathbf{z}, \boldsymbol{\rho}; \theta_G), \boldsymbol{\rho}; \theta_D)] \quad (2)$$

The beauty of the GAN is that the generated images are never compared directly with any of the training images. The generator therefore learns a *smooth* distribution of realistic faces from which new identities can be sampled.

3.2. Intra-class variation isolation

In order to control some attribute of a generated image in a continuous fashion, for example the pose seen in a face-image, a typical C-GAN would require each training image

to be labeled with a precise and accurate pose-estimation. For our method, intra-class variation isolation (IVI), precise continuous labels are not required. Nevertheless, the IVI-GAN is still able to learn models with disentangled sources of variation that are continuously adjustable via semantically meaningful parameters.

The IVI-GAN uses only binary labels. In a typical C-GAN with binary labels as input to the generator, the presence of a particular attribute would be specified via a one-hot vector. This would cause the generator to switch domains (perhaps from generating non-smiling facial images to smiling ones) and to re-purpose the elements of the random latent vector, \mathbf{z} , in whichever way it might prefer to do so. Variation within those attribute categories would then be controlled in some unknown way by the combination of all random values in the input vector. For example, how would one control the type of smile? Should the person be laughing, content, or smug? Via intra-class variation isolation, we are able to easily control this variation via sets of disentangled parameters. The trick is, rather than providing binary attribute-labels to the generator and having it switch to generating images from a different domain, we instead provide additional sources of variation that the generator can use to represent the additional variation due to the presence of that attribute.

The additional sources of variation might be individual random parameters or they might be vectors of random parameters depending on how many modes of variation you expect to find or wish to control within each attribute-category. If the attribute label (selected at random from the real data distribution) were 0, then each element of the corresponding parameter-vector would also be set to 0 in order to prevent those parameters being used to control variation not associated with that attribute. One way to look at it is that we have replaced binary attribute-labels with either zero or non-zero vectors on input to the generator. However, when the vector is non-zero, variation can be derived from within the ‘‘label-vector’’ itself. For control of the attribute to work well, there should be little variation of the attribute among the training images labeled with zeros. For example, if the relevant attribute were lighting then one might label all images containing ambient lighting with zeros. To be classified as real, generated images labeled with zeros must also appear to be ambiently lit. Information about specific characteristics of the generated ambient image (in this case including the intensity and colour of ambient light) is necessarily derived from \mathbf{z} since $\boldsymbol{\rho}$ is set to all zeros. However, generated images labeled with ones must contain stronger lighting conditions in order to appear real to the discriminator. In this case, information about specific characteristics in the image (now including lighting direction; the number of lights; etc.) can be derived from \mathbf{z} or $\boldsymbol{\rho}$. However, it makes sense for the C-GAN to assign control to $\boldsymbol{\rho}$ only

since setting ρ to zero must switch off the lights and return the image to ambient. Information about nothing other than non-ambient lighting should be present in ρ since the generator cannot rely on it being available to use. It is only available to use when the image should be more strongly lit. In this way the parameters ρ become semantically disentangled from \mathbf{z} .

The attributes controlled by ρ need not be mutually exclusive provided the dataset contains examples of each attribute disjoint from the others individually. (For example, in order to disentangle pose and expression, there must exist images where the expression parameter vector is isolated from the pose parameter vector, such as images containing non-neutral expressions at frontal poses. In these cases, the pose parameter vectors would be set to all zeros and the generator would learn that it is only consistently able to derive variation from the expression vectors with which it can control the precise form of the non-neutral expressions in the images.) This allows the learning of complete models with multiple controllable properties. For example, the method could be used to learn a realistic face model with controllable pose, expression, lighting and age. The remaining parameters, \mathbf{z} , would hence mostly represent the identity but also the uncontrolled sources of variation such as the background.

Technically, the changes to the standard C-GAN are very simple and involve modifying only the form of the labels provided to the GAN. The function to be minimised to train the IVI-GAN’s discriminator is

$$\mathcal{L}_{\theta_D} = \mathbb{E}_{(\mathbf{x}, \mathbf{y}) \sim p_{data}} [D(\mathbf{x}, \mathbf{y}; \theta_D)] - \mathbb{E}_{\mathbf{z} \sim \mathcal{N}, \beta \sim p_{data}} [D(G(\mathbf{z}, \rho; \theta_G), \beta; \theta_D)] \quad (3)$$

where $\mathbf{y} \in \{0, 1\}^n$ are now binary labels for n categories, and $\beta \in \{0, 1\}^n$ are binary labels sampled from the same distribution as \mathbf{y} (but, as previously, do not necessarily correspond). The novel aspect of the loss is the way in which the random parameters, ρ , are chosen.

$$\rho = \begin{bmatrix} \mathbf{p}_1 \\ \mathbf{p}_2 \\ \vdots \\ \mathbf{p}_n \end{bmatrix} \text{ where } \mathbf{p}_i \in \begin{cases} \mathcal{N}^{q_i}, & \text{if } \beta_i = 1 \\ \mathbf{0}^{q_i}, & \text{if } \beta_i = 0 \end{cases} \quad (4)$$

Here $\mathbf{0}^{q_i}$ is a zero-vector of length q_i . Analogous to the C-GAN, the function then minimised to train the generator is

$$\mathcal{L}_{\theta_G} = \mathbb{E}_{\mathbf{z} \sim \mathcal{N}, \beta \sim p_{data}} [D(G(\mathbf{z}, \rho; \theta_G), \beta; \theta_D)] \quad (5)$$

Figure 2 depicts a C-GAN with our IVI modifications highlighted.

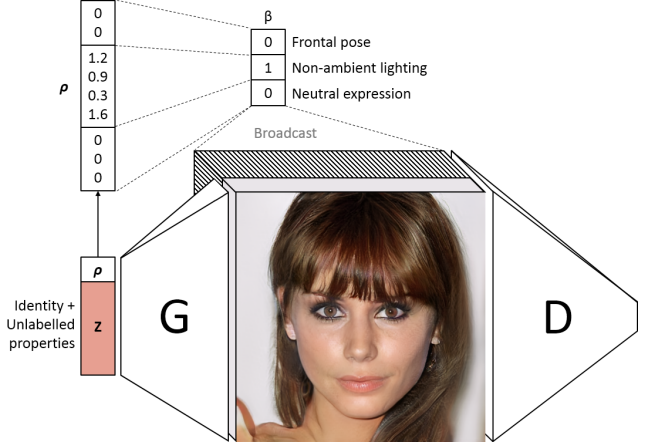


Figure 2. Illustration of the concept of intra-class variation isolation in the generator loss part of the IVI-GAN; i.e. equation (5).

4. Implementation

Our implementation is built upon the stable and efficient progressive GAN of [15], a Tensorflow implementation of which was made publicly available by Nvidia. The progressive GAN begins by generating images of 4x4 resolution and then progressively fades in new convolutional upscaling layers until the desired resolution is reached. There has been much recent work on improving the quality of GAN output published in the literature. We tested a selection of these enhancements and found that our best results were produced by a progressive Wasserstein GAN with the standard gradient penalty (GP) term of [13] where the weight of the GP term was allowed to evolve throughout training based on an *adaptive lambda* scheme similar to that in [5]. (Details of this scheme can be found in Appendix A.) In the generator we use orthogonal initialisation of weights and replace the pixel-wise feature normalisation used in [15] with the orthogonal regularisation of [4] using the suggested weight of 0.0001. Fréchet Inception Distances calculated for these tests are presented in Table 1.

4.1. Conditioning the GAN

The way in which labels and label-parameters are used to condition GANs is an open area of research. For example, [19] finds that, given certain assumptions about the form of the distribution of data, the optimal method of conditioning the discriminator should be to learn some inner-product of the label-vector with the channels at each pixel; in [9] the generator network is conditioned via instance-normalisation parameters. We have used the more straightforward method of concatenating label-vectors with inputs but expect that these more sophisticated methods of conditioning may be used to improve results. We concatenate our *categorical variation-isolating* label-parameter vector,

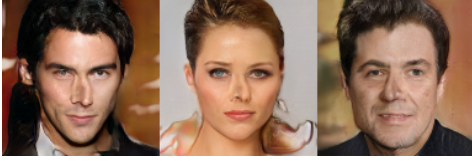


Figure 3. Examples of problematic broken nose features generated by an IVI-GAN with auxiliary classifier.

ρ , with the random vector on input to the generator, and on input to the discriminator we concatenate the binary labels, y and β , as additional channels repeated at each pixel of the real and generated images respectively.

An analysis of where best to concatenate conditioning vectors was performed in [21]. They predicted that earlier in the network should be better since the discriminator would be afforded more learning interactions with the information. In fact they conclude that it is best to concatenate the conditioning with the first hidden layer. However, in a progressive architecture the first convolutional layer of the discriminator is not faded in until the final stages of training. In our case, it therefore makes more sense to concatenate the conditioning with the image where it is then scaled down and fed to each layer of the progressive network as they are being faded in. Ultimately, once all layers of the progressive discriminator are active, the conditioning information is only presented to the discriminator at the very start.

Many applications make use of auxiliary classifiers (ACs) [20] as a way of ensuring that conditional parameters not be ignored during generation of images. We tested this method in conjunction with IVI-GAN using the auxiliary classifier already implemented in Nvidia’s progressive GAN code. However, we found results to be unsatisfactory. As noted in [18], auxiliary classifiers encourage the generator to produce images that are easy to classify; a goal which is not in alignment with the principal goal of the GAN: to generate samples indistinguishable from real data. We found that, given a large weight in the discriminator loss, the AC-term caused mode-collapse, squeezing variation into narrow, well-separated categories. For example, upon varying continuous conditional pose parameters we observed a discrete jump in the generated pose between frontal and large poses. Giving less weight to the AC-term ameliorates the discrete jumps in pose. However, more subtle artifacts remained, such as broken noses pointing in one direction or the other; a feature obviously used by the discriminator to help identify slightly non-frontal poses. See Figure 3 for examples of this behaviour.

4.2. Constraining the identity

If the datasets of facial images we use to train our IVI-GAN were perfectly balanced, i.e. if they contained equal numbers of images for each possible combination of binary

attributes, our intra-class variation isolation should work well. However, in practice datasets tend not to be well-balanced and there exist, therefore, correlations between image-properties. For example, people tend to smile for the camera but revert to neutral expressions when they are looking away. In order to match the distribution of data correctly, the IVI-GAN may therefore learn to alter the expression upon adjusting the pose. Using unbalanced datasets such as CelebA-HQ which, for example, contains roughly 2/3 females and 1/3 males, we see changes of gender for some of the more extreme parameter values. (See, for example, the fail cases in Figure 4.) Balancing for gender avoids this particular problem. However, more subtle fluctuations in identity are difficult to avoid. This has led us to introduce constraints on the identity. We have tested two forms of constraint: one explicit biometric identity constraint and a second implicit constraint which can be used in the case of learning a model of lighting.

4.2.1 The biometric identity-constraint

To ensure that identity remains constant upon adjusting other image-properties, we have added a term to the generator loss involving a pre-trained biometric network [14] that accepts a facial image as input and produces a 128-dimensional encoding of the identity.

$$\mathcal{L}_{ID} = \mathbb{E}_{\mathbf{z}, \rho, \rho_2 \sim \mathcal{N}} \left[\|B(G(\mathbf{z}, \rho)) - B(G(\mathbf{z}, \rho_2))\|^2 \right] \quad (6)$$

where B is the biometric network and ρ_2 is a second set of random label-parameters. We run the generator twice for the same \mathbf{z} but different ρ and ensure that the identity encodings remain close. (N.B. we have dropped the θ for convenience of notation.) The full generator loss is then

$$\mathcal{L}_{\theta_G} = \mathbb{E}_{\mathbf{z}, \rho, \rho_2 \sim \mathcal{N}} [D(G(\mathbf{z}, \rho), \beta) + \lambda_{ID} \mathcal{L}_{ID}] \quad (7)$$

where λ_{ID} is a hyper-parameter to be tuned.

N.B. this form of ID-constraint may be useful for learning a disentangled model. However, relying on it would limit the success of data augmentation for further improving biometric networks. In the following section we present an alternative form of ID-constraint that doesn’t suffer from this issue of cyclic dependence.

4.2.2 An implicit identity-constraint for lighting

In the case of learning a lighting model, there is a particular property that the model must have which we can constrain and thereby also implicitly constrain the identity. The property of which we speak is that lighting must be additive. For example, the shading in an image of a scene with two light sources is the same as the sum of the shading of the same scene with the two light sources acting on it separately. This

means that we should be able to construct an image containing certain lighting effects by forming a linear combination of two constituent images. We propose, therefore, the following modification to the generator:

$$G_{ave} = \frac{G(\mathbf{z}, \boldsymbol{\rho}) + G(\mathbf{z}, \mathbf{0})}{2} \quad (8)$$

where $\boldsymbol{\rho}$ is now only lighting label-parameters and $\mathbf{0}$ is a vector of zeros the same length as $\boldsymbol{\rho}$ indicating that ambient lighting should be generated. G_{ave} would replace G in both equation (3) and (5). Whereas previously we may have seen small identity-fluctuations in $G(\mathbf{z}, \boldsymbol{\rho})$ compared to $G(\mathbf{z}, \mathbf{0})$, the generator must now avoid these fluctuations in order that the combination of the two images appear realistic to D and not be some blurry, misaligned mess.

5. Results

5.1. State-of-the-art GAN training

As mentioned in Section 4, we performed tests of various GAN-training methods, using the progressive Wasserstein GAN-GP as a baseline. We trained on the CelebA-HQ dataset [15] of 30,000 images up to a resolution of 128x128 and then until the network had seen a total a total of 18 million images. We trained using the default settings and a fade/stabilisation period of 600,000 images meaning that 128x128 resolution was reached after having seen 6 million images. Table 1 shows Fréchet Inception Distances (FIDs) for each GAN-configuration evaluated on 50,000 generated images and compared against the CelebA-HQ training dataset.

Training configuration	FID (50k)
Wasserstein+GP	9.83
Wasserstein+GP+No_MBStd	11.78
Wasserstein+GP+AL	9.64
Wasserstein+GP_max+AL	9.84
Wasserstein+GP+AL (uniform)	10.17
Wasserstein+GP+AL+O.Reg.	9.27
Non-saturating+GP+AL	15.93

Table 1. Fréchet Inception Distances (FIDs) calculated for 50,000 generated images compared to the CelebA-HQ *training* dataset.

We found that removing the mini-batch standard deviation layer and drawing the values of the random latent vector, \mathbf{z} , from a uniform distribution (“No_MBStd” and “uniform” in Table 1) rather than a from standard Gaussian ditribution, deteriorated results. We also found that FID scores are significantly worse when the GAN is trained using the original *non-saturating* GAN-loss of [11]. Our version of the *adaptive-lambda* scheme of [5] (“AL” in Table 1) improved FIDs. However, we found that this was only the case

if gradient norms were regularised across the whole mini-batch, not just in cases where the gradient norm is greater than 1.0 (“GP_max” in Table 1) as was advocated in [5]. Our best results were obtained when regularising the weights of the generator using orthogonal regularisation [4] (“O.Reg.” in Table 1) instead of applying the pixel-wise feature vector normalisation of [15] that was used in the baseline.

We also attempted to replace the gradient penalty with the less computationally expensive spectral normalisation of [18] which is advocated by [16]. However, we found that spectral normalisation leads to vanishing gradients in deep networks such as that being tested here, which has 11 convolutional layers in the discriminator. In [16] we believe this problem was not encountered due to testing shallower networks and ResNet architectures.

5.2. Comparison of IVI-GAN with a classical continuous C-GAN

In this section we investigate the capability of our IVI-GAN, and of a classic continuous C-GAN (CC-GAN), to learn a bijection between parameter space and the semantic spaces of an image; in this case “pose space” and “identity space”. To make the comparison fair, we use the same network architecture as our IVI-GAN. The only modification is the form of the labels provided to the generator and discriminator. As described in Section 3.1, continuous pose labels are randomly selected from the labels of the training dataset and used to directly condition the generator and the discriminator. To condition the generator, a set of labels is concatenated with the random input vector, and to condition the discriminator, labels are tiled and concatenated with the associated image as additional channels.

We trained the two GANs to learn to disentangle the pose attributes (yaw and pitch) due to the ease of verifying pose in the generated images using an internally developed pose detector. The two aspects of the generated images we wish to verify are 1) whether certain values of the pose parameters result in the same pose being generated across different identities, and 2) whether identity is well-constrained at different poses. Results are presented in Tables 2 and 3.

Table 2 shows the mean poses generated for a selection of pose parameters, $\boldsymbol{\rho}$, by our IVI-GAN and by the classic continuous conditional GAN (CC). In this particular case, the IVI-GAN learned to represent pitch-like variation via the first conditional parameter and yaw-like variation via the second. The consistency of generated poses over 100 random identities is good with the maximum measured standard deviation of detected pose vectors from the mean pose vector being 8.8°. For the CC-GAN evaluated at similar poses, the maximum standard deviation was not much smaller at 6.9° despite having had the benefit of being trained with precise labels. Plotting the mean poses for the IVI-GAN (see Appendix B) reveals that the learned axes of

GAN configuration		Mean pose		StdDev pose
Type	ρ	yaw	pitch	
IVI	(0.0, 0.0)	-0.2°	-0.1°	4.4°
	(1.0, 0.0)	-1.6°	-8.8°	5.8°
	(2.0, 0.0)	-2.9°	-15.5°	6.5°
	(3.0, 0.0)	-4.8°	-20.7°	7.6°
	(0.0, 1.0)	10.2°	-1.3°	7.5°
	(0.0, 2.0)	23.8°	-6.5°	8.8°
	(0.0, 3.0)	33.7°	-12.6°	8.8°
CC	(0.0°, 0.0°)	-0.2°	0.6°	3.8°
	(-1.6°, -8.8°)	-2.0°	-7.3°	4.3°
	(-2.9°, -15.5°)	-2.9°	-14.6°	3.9°
	(-4.8°, -20.7°)	-5.1°	-19.4°	4.5°
	(10.2°, -1.3°)	9.3°	0.8°	4.8°
	(23.8°, -6.5°)	23.5°	-5.2°	6.3°
	(33.7°, -12.6°)	32.5°	-11.4°	6.9°
IVI + \mathcal{L}_{ID}	(0.0, 0.0)	-0.7°	0.2°	7.0°
	(1.0, 0.0)	-10.0°	0.8°	8.6°
	(2.0, 0.0)	-21.3°	-1.0°	9.9°
	(3.0, 0.0)	-30.4°	-3.3°	9.9°
	(0.0, 1.0)	-4.0°	-4.7°	8.6°
	(0.0, 2.0)	-8.5°	-9.6°	10.1°
	(0.0, 3.0)	-13.6°	-14.4°	10.6°

Table 2. Evaluation of the consistency of generated poses. The mean yaw and pitch values, and standard deviation of the pose direction vector were calculated over 100 random identities for the given label-configurations. Note that the ρ fed to the IVI-GANs are abstract latent variables and not specifications of the desired pose as for the CC-GAN.

variation are roughly orthogonal. However, there is some correlation at larger values. Nevertheless, the goal of IVI is not to disentangle parameters of the same type from each other, but to disentangle them from the parameter sets of different attributes and from the identity. An extension of this analysis can be found in Appendix B.

Table 3 shows face-matching scores between images synthesised at pose and the frontal image synthesised using the same random latent vector, averaged over 100 random identities. At each roughly equivalent pose, e.g. $\rho_{IVI} = (1.0, 0.0)$ c.f. $\rho_{CC} = (-1.6^\circ, -8.8^\circ)$, the mean matching score for the CC-GAN is better than for the IVI-GAN indicating that identity is better preserved across poses. For both GANs, however, the matchings are, on average, considered to be failures by typical standards at larger values of pose. This indicates the need for additional constraints on the identity during training. In Section 5.3 we evaluate two such constraints.

5.3. ID-constrained intra-class variation isolation

Figure 4 shows a selection of images generated by the IVI-GAN trained for the experiment of the previous sec-

GAN configuration		Mean matching score	StdDev score
Type	ρ		
IVI	(1.0, 0.0)	5720.7	1388.1
	(2.0, 0.0)	2723.2	770.2
	(3.0, 0.0)	1920.7	352.4
	(0.0, 1.0)	5457.1	1242.1
	(0.0, 2.0)	2777.8	715.4
	(0.0, 3.0)	2039.1	417.5
	CC	(-1.6°, -8.8°)	6478.5
(-2.9°, -15.5°)		3920.8	963.4
(-4.8°, -20.7°)		2810.9	721.1
(10.2°, -1.3°)		5550.8	1016.9
(23.8°, -6.5°)		2656.3	525.8
(33.7°, -12.6°)		2113.2	393.2
IVI + \mathcal{L}_{ID}	(1.0, 0.0)	7738.5	1245.3
	(2.0, 0.0)	4780.0	941.4
	(3.0, 0.0)	3520.3	802.0
	(0.0, 1.0)	9517.2	1021.0
	(0.0, 2.0)	6304.4	1197.6
	(0.0, 3.0)	4456.2	988.6

Table 3. Evaluation of the consistency of generated identity with changing pose. The mean and standard deviation face-matching scores were calculated over 100 random identities synthesised using the given pose-parameters. Matchings were performed against the frontalised identities with $\rho = (0.0, 0.0)$. Matchings considered to be failures (score < 3000) are indicated in red.

tion. As you can see by comparing the sets of images in each row, the identity changes as the pitch-like parameter is modified. To attempt to avoid such problems, we trained an IVI-GAN with the additional biometric ID-constraint described in Section 4.2.1. The biometric network [14] was pre-trained on images of resolution 96x96 and so we only fade in the additional ID-loss during the final stabilisation period of the training of the progressive GAN. We gradually adjust λ_{ID} from 0.0 to 0.0001 over an epoch of 30,000 images. Figures 5 and 6 show the effect of adjusting the yaw-like parameter and the pitch-like parameter respectively. Comparison of Figures 6 and 4 show that the ID-constraint significantly improves the quality of results.

Quantitative analysis of the effect of the ID-constraint is given in the rows labeled IVI+ \mathcal{L}_{ID} in Tables 2 and 3. We see that the ability of the network to generate images at large poses seems to become slightly restricted with maximum observed values of yaw and pitch of -30.4° and -14.4° compared to 33.7° and -20.7° for the IVI-GAN without ID-constraint. Bear in mind, however, that the parameter values for the two instances of the IVI-GAN are not strictly comparable since different models of pose have been learned. The ID-constraint also seems to cause the learned axes of variation to be less orthogonal and for poses to be less consistently generated. On the other hand, Ta-



Figure 4. Images analogous to those in Figure 6 but with no constraint on the identity. Each row of images was generated using the same identity vector. However, as the pitch is varied, the identity morphs towards other genders. We believe this is due to an unbalanced dataset and insufficient identity variation among images with large values of pitch.

ble 3 shows that, on average, all generated images for the given parameter settings match well with their frontal counterparts, with the lowest mean matching score being 3520.3 at an average pose of $(-30.4^\circ, -3.3^\circ)$. Note that the biometric network used to produce these matching scores was not the same as that used to constrain the IVI-GAN.

In Figure 1 we present a selection of images generated by an IVI-GAN trained with only our novel additive lighting constraint; i.e. the explicit biometric ID-constraint was not applied. We trained on a 100k subset of CelebA in combination with a set of binary lighting labels indicating whether the subject of the image is ambiently or non-ambiently lit. Removing the softmax layer of our lighting classifier gives an heuristic for the strength of lighting in the images. In selecting the 100k subset of CelebA, we chose 50k of the images with the largest probability of not being ambient to ensure adequate lighting variation in the dataset. Comparing images in each row of Figure 1 shows that the identity is well constrained for different lighting conditions. This is thanks to the modified generator in equation (8) requiring that features in the ambient and non-ambient constituent images remain generally aligned. By comparing images in each column of Figure 1 we can see that the effect of each set of lighting parameters remains semantically similar for different identities.

Additional results can be found in Appendix C. We have also prepared a video demonstrating the smooth, semantically separated image alterations possible using our ID-constrained IVI-GAN. This can be viewed at <https://youtu.be/hoWOFeADwdY>.

6. Conclusions

We have shown that it is possible to adapt a conditional GAN in order to gain continuous control over image attributes without the need for extensive labeling. Only sim-



Figure 5. Images generated using intra-class variation isolation and the explicit biometric ID-constraint. Here the first parameter of ρ has learned to represent the yaw component of variation in non-frontal images. Left-hand column: $\rho = (-2.0, 0.0)$; Central column: $\rho = (0.0, 0.0)$; Right-hand column: $\rho = (2.0, 0.0)$. (See also Figure 6.)



Figure 6. Images generated using intra-class variation isolation and the explicit biometric ID-constraint. Here the second parameter of ρ has learned to represent a pitch-like component of variation in non-frontal images. Left-hand column: $\rho = (0.0, -2.0)$; Central column: $\rho = (0.0, 0.0)$; Right-hand column: $\rho = (0.0, 2.0)$.

ple binary labels, indicating whether an attribute is present in one form or another, are required. The GAN is allowed to discover its own way of modeling the variation present in that attribute in an unsupervised fashion and control over the attribute is assigned to semantically separated input parameters via our intra-class variation isolation mechanism. To the best of our knowledge, IVI-GAN is the first network to achieve this separation in a weakly supervised manner. A novel, physically motivated constraint on the GAN’s generator was also introduced and can be applied when learning models of lighting in images in order to better constrain the identity. In conjunction with our intra-class variation isolation method, this constraint has been shown to be highly successful. Potential applications of IVI-GAN include dataset-augmentation and image-manipulation.

References

- [1] M. Arjovsky, S. Chintala, and L. Bottou. Wasserstein generative adversarial networks. In D. Precup and Y. W. Teh, editors, *Proceedings of the 34th International Conference on Machine Learning*, volume 70 of *Proceedings of Machine Learning Research*, pages 214–223, International Convention Centre, Sydney, Australia, 06–11 Aug 2017. PMLR. [2](#), [3](#)
- [2] J. Bao, D. Chen, F. Wen, H. Li, and G. Hua. Towards open-set identity preserving face synthesis. In *The IEEE Conference on Computer Vision and Pattern Recognition (CVPR)*, June 2018. [2](#)
- [3] A. Brock, J. Donahue, and K. Simonyan. Large scale gan training for high fidelity natural image synthesis. *CoRR*, abs/1809.11096, 2018. [2](#)
- [4] A. Brock, T. Lim, J. M. Ritchie, and N. Weston. Neural photo editing with introspective adversarial networks. In *International Conference on Learning Representations*, 2017. [2](#), [4](#), [6](#)
- [5] Y.-S. Chen, Y.-C. Wang, M.-H. Kao, and Y.-Y. Chuang. Deep photo enhancer: Unpaired learning for image enhancement from photographs with gans. In *The IEEE Conference on Computer Vision and Pattern Recognition (CVPR)*, June 2018. [4](#), [6](#), [10](#)
- [6] Z. Chen, S. Nie, T. Wu, and C. G. Healey. High resolution face completion with multiple controllable attributes via fully end-to-end progressive generative adversarial networks. *CoRR*, abs/1801.07632, 2018. [2](#)
- [7] Y. Choi, M. Choi, M. Kim, J.-W. Ha, S. Kim, and J. Choo. Stargan: Unified generative adversarial networks for multi-domain image-to-image translation. In *The IEEE Conference on Computer Vision and Pattern Recognition (CVPR)*, June 2018. [2](#)
- [8] C. Donahue, A. Balsubramani, J. McAuley, and Z. C. Lipton. Semantically decomposing the latent spaces of generative adversarial networks. In *International Conference on Learning Representations*, 2018. [2](#)
- [9] V. Dumoulin, J. Shlens, and M. Kudlur. A learned representation for artistic style. In *International Conference on Learning Representations*, 2017. [4](#)
- [10] E. Friesen and P. Ekman. Facial action coding system: a technique for the measurement of facial movement. *Palo Alto*, 1978. [3](#)
- [11] I. Goodfellow, J. Pouget-Abadie, M. Mirza, B. Xu, D. Warde-Farley, S. Ozair, A. Courville, and Y. Bengio. Generative adversarial nets. In Z. Ghahramani, M. Welling, C. Cortes, N. D. Lawrence, and K. Q. Weinberger, editors, *Advances in Neural Information Processing Systems 27*, pages 2672–2680. Curran Associates, Inc., 2014. [1](#), [6](#)
- [12] G. Gu, S. T. Kim, K. H. Kim, W. J. Baddar, and Y. M. Ro. Differential generative adversarial networks: Synthesizing non-linear facial variations with limited number of training data. *CoRR*, abs/1711.10267, 2017. [2](#)
- [13] I. Gulrajani, F. Ahmed, M. Arjovsky, V. Dumoulin, and A. C. Courville. Improved training of wasserstein gans. In I. Guyon, U. V. Luxburg, S. Bengio, H. Wallach, R. Fergus, S. Vishwanathan, and R. Garnett, editors, *Advances in Neural Information Processing Systems 30*, pages 5767–5777. Curran Associates, Inc., 2017. [2](#), [3](#), [4](#)
- [14] M. A. Hasnat, J. Bohné, J. Milgram, S. Gentric, and L. Chen. Deepvisage: Making face recognition simple yet with powerful generalization skills. In *ICCV Workshops*, pages 1682–1691, 2017. [1](#), [5](#), [7](#)
- [15] T. Karras, T. Aila, S. Laine, and J. Lehtinen. Progressive growing of GANs for improved quality, stability, and variation. In *International Conference on Learning Representations*, 2018. [2](#), [4](#), [6](#)
- [16] K. Kurach, M. Lucic, X. Zhai, M. Michalski, and S. Gelly. The gan landscape: Losses, architectures, regularization, and normalization. *CoRR*, abs/1807.04720, 2018. [6](#)
- [17] M. Mirza and S. Osindero. Conditional generative adversarial nets. *CoRR*, abs/1411.1784, 2014. [1](#), [3](#)
- [18] T. Miyato, T. Kataoka, M. Koyama, and Y. Yoshida. Spectral normalization for generative adversarial networks. In *International Conference on Learning Representations*, 2018. [2](#), [5](#), [6](#)
- [19] T. Miyato and M. Koyama. cGANs with projection discriminator. In *International Conference on Learning Representations*, 2018. [4](#)
- [20] A. Odena, C. Olah, and J. Shlens. Conditional image synthesis with auxiliary classifier GANs. In D. Precup and Y. W. Teh, editors, *Proceedings of the 34th International Conference on Machine Learning*, volume 70 of *Proceedings of Machine Learning Research*, pages 2642–2651, International Convention Centre, Sydney, Australia, 06–11 Aug 2017. PMLR. [5](#)
- [21] G. Perarnau, J. van de Weijer, B. Raducanu, and J. M. Álvarez. Invertible conditional gans for image editing. *CoRR*, abs/1611.06355, 2016. [5](#)
- [22] A. Pumarola, A. Agudo, A. M. Martínez, A. Sanfeliu, and F. Moreno-Noguer. Ganimation: Anatomically-aware facial animation from a single image. *CoRR*, abs/1807.09251, 2018. [2](#), [3](#)
- [23] D. Sáez Trigueros, L. Meng, and M. Hartnett. Generating photo-realistic training data to improve face recognition accuracy. *arXiv preprint arXiv:1811.00112*, 2018. [2](#)
- [24] L. Tran, X. Yin, and X. Liu. Disentangled representation learning gan for pose-invariant face recognition. In *The IEEE Conference on Computer Vision and Pattern Recognition (CVPR)*, July 2017. [2](#)

Appendix A. The adaptive λ_{GP} scheme

As shown in Table 1, our best results are for GANs trained using an adaptive-lambda scheme similar to that of [5]. In [5] a moving average of the L2-norm of the gradients of the discriminator output with respect to image pixel values is maintained. If this moving average passes above or below certain values, the weight of the Wasserstein GAN’s gradient penalty (GP) term is doubled or halved (respectively). The moving average is calculated over a sliding window of 50 discriminator iterations and the window of permitted gradient-norm values is set to [1.001, 1.05].

We found that we needed to modify this scheme slightly since gradient norms at the start of training can be small causing λ_{GP} to be continually halved until it eventually underflows to zero and can then not be re-inflated by doubling when necessary. We avoid this problem by adding and subtracting an increment rather than doubling or halving. We use the same window of permitted gradient-norm values as [5], an initial value of $\lambda_{GP} = 10$, and an increment of 0.1. For ease of implementation, rather than storing a moving window of 50 gradient-norm values, we instead keep an exponential moving average with a decay rate of 0.9.

$$\mu_i = 0.9\mu_{i-1} + 0.1 \|\nabla_{\mathbf{x}} D(\mathbf{x})\|^2 \quad (9)$$

$$\lambda_{GP} = \begin{cases} \lambda_{GP} + 0.1, & \text{if } \mu_i > 1.05 \\ \lambda_{GP} - 0.1, & \text{if } \mu_i < 1.001 \text{ and } \lambda_{GP} - 0.1 \geq 0 \\ 0, & \text{otherwise} \end{cases} \quad (10)$$

Appendix B. Detailed comparison of learned pose models

Results in this section complement those of Section 5.2. We investigate the effect of conditional pose parameters on the poses detected in generated images for the classic continuous C-GAN (CC-GAN) and on our IVI-GAN both with and without ID-constraint.

The red and blue points in Figures 7, 8 and 9 show detected poses for various parameter configurations averaged over 100 different identities. Some of the configurations are those shown in Table 2. However, we have extended the experiments to cover more of the space. In Figure 7 the configurations shown in red test the effect of each pose parameter separately in increments of 10° between -40° and 40° with the other parameter set to 0° . The configurations shown in blue test the effect of varying both parameters simultaneously; i.e. parameters are varied linearly in the ranges $(-40^\circ, -40^\circ)$ to $(40^\circ, 40^\circ)$, and $(-40^\circ, 40^\circ)$ to $(40^\circ, -40^\circ)$, again in increments of 10° . The grey circles in Figure 7 show detected poses (no averaging) in generated images for 500 sets of pose parameters selected from a random uniform distribution in the ranges $[-60, 60]$ for yaw

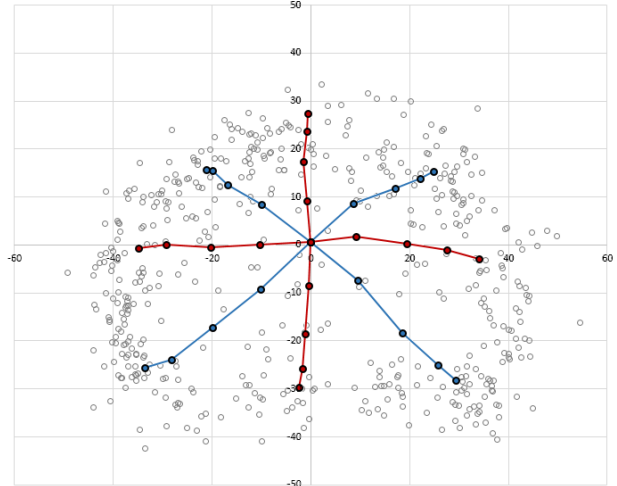


Figure 7. Detected poses in images generated by a continuous C-GAN. Red and blue points indicate mean values of detected pose for a selection of specified parameter values, averaged over 100 identities. Grey circles indicate detected poses for a random uniform sampling of parameter values.

and $[-50, 50]$ for pitch. Our intention is to show the range of poses that it is possible to generate.

Generated poses in Figure 7 seem to stay close to their intended axes of variation. Notice, however, that the space between points decreases as the parameter values are increased. This indicates that the generator is not able to stay faithful to the conditioning labels at larger values of pose, probably because there are not enough images available at those poses for the generator to have learned to model them. This is also the reason that the cloud of grey circles forms a halo shape. Rather than very large-pose images being generated, larger parameter values have instead led to poses of around 30° to 40° in magnitude being generated.

Figures 8 and 9 show results analogous to those in Figure 7 but for the IVI-GAN and the IVI-GAN+ID-constraint respectively. For the red and blue points, parameters were selected in a similar way but in the ranges $[-4, 4]$ at intervals of 1. (Remember that the GANs were trained with parameters randomly selected from a standard Gaussian distribution, not with labels.) Parameters used to generate the images represented by the grey circles were selected from a random uniform distribution within the range $[-6, 6]$ for both yaw and pitch.

Without the constraint of pose-labels, the generators of the two IVI-GANs have learnt to model pose in a way that is affected non-orthogonally by the two parameters. The clouds of grey circles show that, although the parameters are entangled with each another, the models span a similar region of *pose-space* as the CC-GAN’s model, at least in the yaw direction.

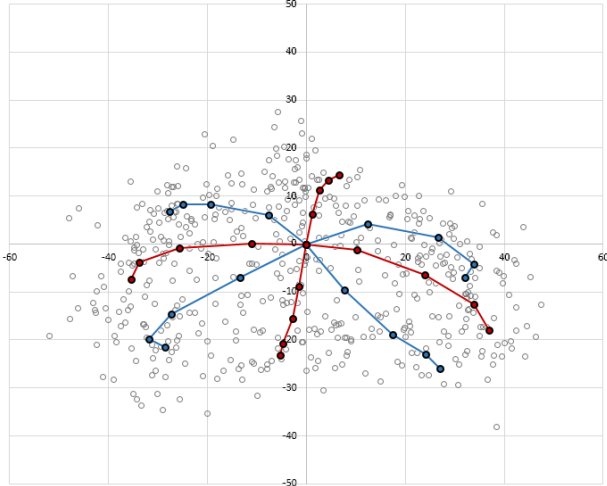


Figure 8. Detected poses in images generated by an IVI-GAN. Red and blue points indicate mean values of detected pose for a selection of specified parameter values, averaged over 100 identities. Grey circles indicate detected poses for a random uniform sampling of parameter values.

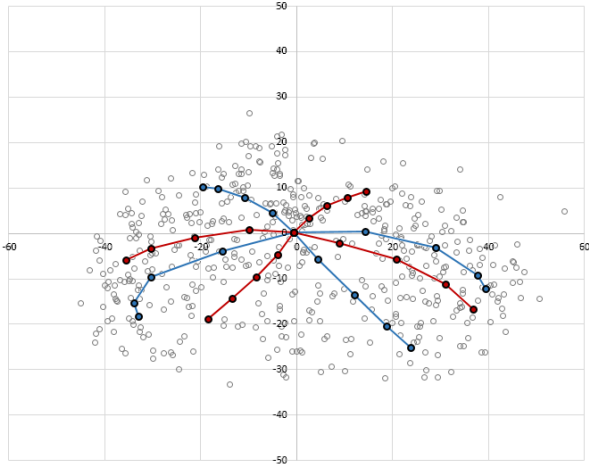


Figure 9. Detected poses in images generated by an IVI-GAN with ID-constraint. Red and blue points indicate mean values of detected pose for a selection of specified parameter values, averaged over 100 identities. Grey circles indicate detected poses for a random uniform sampling of parameter values.

The detected poses plotted in grey in Figures 7-9 were generated from parameters drawn from uniform distributions. We did this to try to show the full spread and upper limits of pose that it is possible to generate. However, the GANs were not trained using uniform parameters and so the plotted distributions contain peculiarities such as the halo shape in Figure 7 and a potential *cut-off* in Figures 8 and 9 where we have limited parameter values to ± 6 , although

Experiment	Mean pose		StdDev pose	
	yaw	pitch	yaw	pitch
CelebA-HQ	-1.3°	-1.2°	11.5°	8.4°
CC-GAN	-2.2°	-1.5°	11.8°	8.3°
IVI-GAN	-0.1°	-0.9°	11.5°	8.5°
IVI-GAN+ID	-0.1°	-1.6°	12.0°	7.9°

Table 4. Statistics of poses detected in CelebA-HQ and in sets of 500 images generated by three GANs with input parameters selected from their respective training distributions.

this second effect should be minimal. Table 4 presents statistics for poses detected in CelebA-HQ and in sets of generated images where the parameters were selected from the distributions used during training; i.e. for the CC-GAN we randomly selected 500 sets of pose labels from those detected for CelebA-HQ, and for the IVI-GANs, parameters were selected from standard normal distributions. The table shows that differences in the statistics from the CelebA-HQ ground-truth are not large. For the IVI-GAN+ID-constraint, the variation in pitch is slightly reduced compared to the other GAN configurations. This is probably the effect of the ID-constraint in combating the significant changes in identity with pitch that can be seen in Figure 4. On the other hand, the variation in yaw is increased for IVI-GAN+ID-constraint; perhaps due to the fact that the slight bias in the mean yaw angle observed for the CelebA-HQ dataset is not present; although this effect did not manifest for the IVI-GAN (without ID-constraint) for which the bias in yaw was also not seen.

Appendix C. Additional results

This section presents additional images generated by IVI-GAN trained with *both* forms of ID-constraint applied simultaneously; i.e. both the biometric constraint described in Section 4.2.1, and the additive lighting constraint described in Section 4.2.2. The network was trained on 100k images taken from CelebA with the following conditional parameter configuration: Gender - 1 parameter (binary); pose - 2 parameters (Gaussian); illumination - 4 parameters (Gaussian); expression - 2 parameters (Gaussian); age - 1 parameter (Abs(Gaussian)); glasses - 2 parameters (Gaussian normalised to unit vector). Each of Figures 10 to 17 show images generated for four random latent vectors, \mathbf{z} (columns), and for either three or four specified parameter vectors, $\boldsymbol{\rho}$ (rows).

Figures 10 and 11 show additional lighting results. For the top rows in each figure, $\boldsymbol{\rho}_{lighting} = \mathbf{0}$, indicating ambient lighting. Comparing images horizontally shows that the effect of the parameters is similar but not identical for each identity. Comparing images vertically reveals that identities are well maintained as $\boldsymbol{\rho}$ is varied.



Figure 10. Additional results: Lighting (male).



Figure 11. Additional results: Lighting (female).

Figures 12 and 13 show the effect of varying one of the expression parameters. The IVI-GAN was allowed two parameters with which to capture the additional variation within the “smile”-labeled images of the CelebA dataset. However, the behaviour of the two parameters was almost identical, presumably because most of the non-smile expression variation is contained in the training images la-



Figure 12. Additional results: Expression (male).



Figure 13. Additional results: Expression (female).

belled as “neutral” (not smiling). Again, for the top row of each of the Figures, $\rho_{expression} = 0$, this time indicating “No smile”. For the second row, the parameter value is 1.0; for the third row, the parameter value is 2.0. The effect of the parameter is similar for each identity and identities remain consistent as ρ is varied.

Figures 14 and 15 show the effect of varying the age parameter. We flipped the “Young” label of CelebA so that the network would learn to use the parameter to capture the additional variation present in images of *older* people. During training, the random parameter was drawn from a *positive only* Gaussian distribution; i.e. values were drawn from a Gaussian distribution but then the absolute value was taken so that the parameter would only vary in the positive direction. For the top rows of Figures 14 and 15, $\rho_{age} = 0$, this time indicating “Young”. Parameter values for the first and second rows are 1.0 and 2.0. The extent of the aging



Figure 14. Additional results: Age (male).



Figure 15. Additional results: Age (female).

appears to be similar across identities. In Figure 14, the identities appear to be well maintained with age; In Figure 15 the identities seem to be less well maintained, although it is quite difficult to judge.

Figures 16 and 17 show the effect of varying the glasses parameters. We used the “Eyeglasses” attribute label of the CelebA dataset and allowed two of the IVI-GAN’s conditional parameters to learn the variation. During training, the two parameters were drawn randomly from a standard Gaussian distribution. However, the 2-vector was then normalised to be of unit length. This was done due to the discrete nature of this particular source of variation. We intended for the absence of a unit vector to indicate “No glasses”, which is indeed the case, (see the first rows of Figures 16 and 17) and we intended for the direction of the vector to indicate the style of glasses. The style of glasses can indeed be controlled. (See the second and third rows of



Figure 16. Additional results: Glasses (male).



Figure 17. Additional results: Glasses (female).

Figures 16 and 17.) However, it is also possible to specify directions for which no glasses are present. This leads to glasses being unrealistically faded out, which is the problem we had hoped to avoid by introducing normalisation of the parameter-vector. (The problem can be seen in the video, linked below, during the transition between normal glasses and sunglasses.) The reason for this issue could be

that the style of glasses is actually discrete in nature, with no realistic-looking “hybrid styles” to bridge gaps (or at least it appears that way to the discriminator based on the training images, of which there are relatively few containing subjects wearing glasses). The final rows of Figures 16 and 17 shows sunglasses with lighting enabled. Notice how this causes realistic translucency effects in the lenses of the glasses.

The majority of results in this supplementary section were taken from the video available at <https://youtu.be/hoWOFeADwdY> which demonstrates smooth transitions between states.